PAPER • OPEN ACCESS

Compact fusion energy based on the spherical tokamak

To cite this article: A. Sykes *et al* 2018 *Nucl. Fusion* **58** 016039

OPEN ACCESS
IOP Publishing | International Atomic Energy Agency
Nuclear Fusion
Nucl. Fusion **58** (2018) 016039 (9pp)
https://doi.org/10.1088/1741-4326/aa8c8d

Compact fusion energy based on the spherical tokamak

A. Sykes[1], A.E. Costley[1], C.G. Windsor[1], O. Asunta[1], G. Brittles[1], P. Buxton[1], V. Chuyanov[1], J.W. Connor[1], M.P. Gryaznevich[1], B. Huang[1], J. Hugill[1], A. Kukushkin[2,3], D. Kingham[1], A.V. Langtry[1], S. McNamara[1], J.G. Morgan[4], P. Noonan[1], J.S.H. Ross[1], V. Shevchenko[1], R. Slade[1] and G. Smith[1,5]

[1] Tokamak Energy Ltd, Culham Science Centre, Abingdon, OX14 3DB, United Kingdom
[2] NRC 'Kurchatov Institute', Kurchatov Sq.1, 123182 Moscow, Russian Federation
[3] MRNU MEPhI, Kashirskoje Ave. 31, 115409 Moscow, Russian Federation
[4] Culham Electromagnetics Ltd, Culham Science Centre, Abingdon, OX14 3DB, United Kingdom
[5] Department of Materials, University of Oxford, 16 Parks Road, Oxford OX1 3PH, United Kingdom

E-mail: alan.sykes@tokamakenergy.co.uk

Received 15 December 2016, revised 19 July 2017
Accepted for publication 14 September 2017
Published 29 November 2017

Abstract
Tokamak Energy Ltd, UK, is developing spherical tokamaks using high temperature superconductor magnets as a possible route to fusion power using relatively small devices. We present an overview of the development programme including details of the enabling technologies, the key modelling methods and results, and the remaining challenges on the path to compact fusion.

Keywords: fusion energy, spherical tokamak, high temperature superconductor

(Some figures may appear in colour only in the online journal)

1. Introduction

Since the mid -1980s the spherical tokamak (ST) has been recognized as an important device for fusion research [1–4]. Such devices demonstrate all the main features of high aspect ratio tokamaks but are relatively small and inexpensive to construct. Moreover, research has shown that they have beneficial properties such as operation at high beta [2], can be run at higher elongation [3, 4], and possibly exhibit higher confinement [4], although more data are needed at higher field and lower collisionality to determine this important aspect. Early attempts to design reactors based on STs did not produce convincing designs, and until recently STs have been mainly seen as useful research devices and possibly as neutron sources for component testing. However, recent advances in both tokamak physics and superconductor technology have changed the situation, and relatively small STs operating at high fusion gain are now considered possible. The key physics step is the realization that the power and the device size needed for high fusion gain may be considerably less than previous estimates, while the key technological step is the advent of ReBCO high temperature superconductors (HTS). In addition to operating at relatively high temperatures, HTS can also produce and withstand relatively high magnetic fields: both of these properties are beneficial in the design of magnets for fusion devices especially for STs where space is limited in the central column. Sorbom *et al* [5] have considered the application of HTS to tokamaks of conventional aspect ratio and produced a design for ARC, a fusion power plant slightly greater in size than JET and at considerably higher field. In this paper, we describe the tokamak energy (TE) programme to develop an alternative route to fusion power based on STs constructed using HTS magnets, and the modelling and concept work underway to determine the optimum power and size of an ST/HTS fusion module. This work identifies key aspects in the physics and technology that significantly affect the size, power and feasibility of such a module. In parallel, experimental work is underway addressing these aspects, including

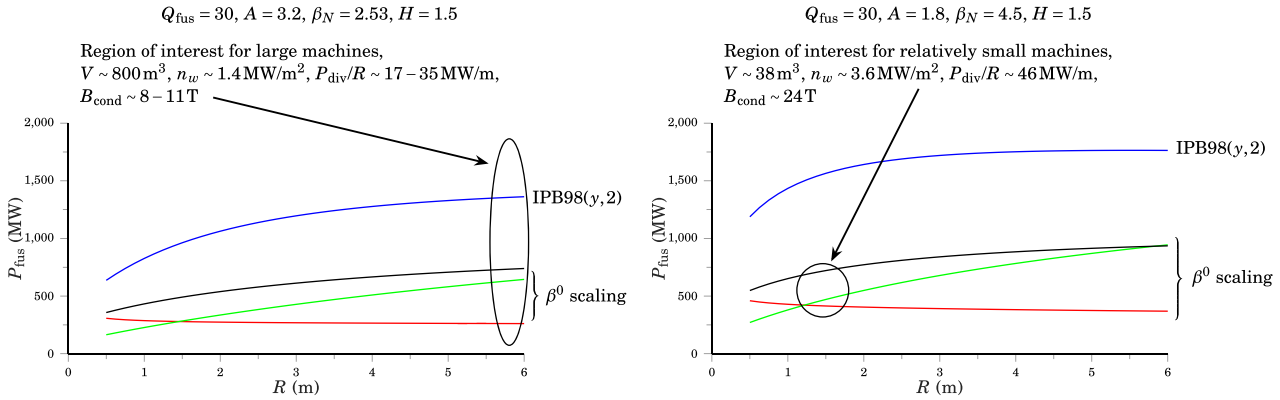

Figure 1. P_{fus} as a function of R_0 at constant $Q_{fus} = 30$, $H = 1.5$ for both IPB98y2 scaling and beta independent scalings for $A = 3.2$ and $A = 1.8$. The values of some key engineering parameters are given in the text in the figure including the field at the conductor on the inboard side, B_{cond}. P_{div} is the transported loss power that has to be handled in the divertor after allowance for radiation losses. Details are given in [6]. The conventional large tokamak solution (left) and the potential low A solutions (right) are indicated. The circled areas show that, with the beta-independent scaling, the wall loads and divertor loads for a relatively small ($R = 1.4$ m) low aspect ratio (1.8) device would be in the range of 3.5 MW m^{-2} and 45 MW m^{-1} respectively, for the same Q_{fus}. This is challenging (although proposals to reduce the divertor load in an ST are described in section 4.2) but in the region of those likely to have to be dealt with in much larger and more powerful devices. The value of B_{cond} is high in the case of the low A approach but potentially achievable using magnets made with HTS (sections 3 and 4).

the construction and operation of a series of STs. In this paper, we present recent new results and the status of the development programme, and we outline the intended next steps.

The paper is divided into five main sections. In section 2 we summarise briefly our earlier modelling work that indicates that there is potentially a solution for a high fusion performance device at relatively small major radius and low aspect ratio. In section 3, we give an overview of the TE development programme; we include a brief description of the STs operated, presently under construction and planned at TE. Our predictions of the performance of a candidate ST fusion module are extended and updated in section 4. Possibilities for modular fusion are discussed briefly in section 5. A summary is given in section 6.

2. Power and size of tokamak pilot plants and reactors

Recent modelling with a system code based on an established physics model has shown that, when operated at reasonable fractions of the density and beta limits, tokamak pilot plants and reactors have a power gain, Q_{fus}, that is only weakly dependent on size; mainly it depends on P_{fus}, and H, where P_{fus} is the fusion power and H is the confinement enhancement factor relative to empirical scalings [6]. Frequently the ITER reference scaling (IPB98y2) is used and H is defined relative to that. When expressed in dimensionless variables this scaling has a significant inverse dependence on the plasma beta, ($\beta^{-0.9}$). However, dedicated experiments on several devices in which the dependence of the confinement time on beta has been probed directly, have shown that the confinement time is almost independent of beta; alternative beta-independent scalings have been developed, for example that by Petty [7]. These scalings are arguably more appropriate because they give consistency between single device and multi-device experiments. Modelling with the system code has shown that the power needed for a given fusion gain is a factor of two to four lower with these scalings (figure 1) [6].

The dependence on P_{fus} implies that it is principally engineering and technological aspects, such as wall and divertor loads, rather than physics considerations, that determine the minimum device size. The lower power requirement arising from the beta-independent scalings is especially advantageous. Using the system code, a wide parameter scan was undertaken to establish possible regions of parameter space that could potentially offer high Q_{fus} with acceptable engineering parameters. In addition to the high aspect ratio, large tokamak solution, a region of parameter space at low aspect ratio and relatively small major radius, and hence small plasma volume, has been identified (figure 1). The physics advantages (such as high beta) of low aspect ratio potentially enable a compact ST module to achieve a high fusion gain at a modest toroidal field (TF) of around 4 T, whereas a compact conventional aspect ratio tokamak requires a very high field on axis ~12 T to achieve high fusion gain—as evidenced by Ignitor [15]. A candidate device (ST135) with a major radius (R_0) of 1.35 m, aspect ratio (A) of 1.8 and magnetic field on axis (B_{T_0}) of 3.7 T operating at $P_{fus} = 185$ MW with a Q_{fus} of 5 was suggested. The study that led to this proposal was mainly a physics study; engineering aspects were not investigated. Some important engineering and technological aspects are currently being developed and key results are presented in this paper (section 4).

3. TE experimental development programme

3.1. HTS

Use of conventional low temperature superconductor (LTS) for an ST fusion device appears impractical because thick shielding ($\geqslant$1 m) would be needed to prevent neutrons heating the superconductor to above 4 K. With shielding of this thickness on the inner central column, the device would be very

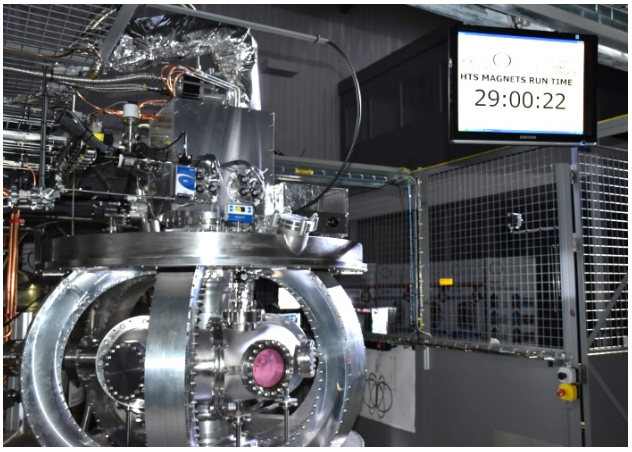

Figure 2. Demonstration of 29 h RF discharge in ST25(HTS) in June 2015. The 6-limb TF magnet is cooled to ~20 K by the Sumitomo cold head shown above the magnet.

large. The advent of HTS, however, potentially provides a solution. HTSs were discovered in the late 1980s and the 2nd generation ReBCO (where Re = Yttrium or Gadolinium) tapes have very promising properties; in particular, they are able to carry high currents under very high magnetic fields. Although superconductivity occurs at around 91 K in zero magnetic field, far better performance is achieved when cooled to around 20–40 K. Thus, for constructing tokamaks, HTS has potentially two advantages relative to LTS: an ability to carry more current at high field, and less demanding cryogenics [8].

3.2. ST25(HTS)

To gain experience with constructing tokamaks using magnets made from HTS, TE constructed a small but complete tokamak (figure 2). This provided the world's first demonstration of a tokamak magnet where all the magnets are made from HTS. All coils (toroidal and poloidal) are wound from YBCO HTS tape. The 6-limb TF cryostat is cooled 'cryo-free' to ~20 K using a single Sumitomo cold head seen above the vessel, thermal conduction from the HTS tape being provided by copper strips; the two poloidal field (PF) coils being cooled by He gas to 20–50 K. A 29 h run was obtained in June 2015, with an RF discharge in hydrogen (figure 2). The TF magnet in ST25(HTS) used a continuous length of 12 mm wide YBCO tape of 48 turns in each of 6 limbs which when operated at 400 A would provide a TF at $R = 0.25$ m of ~0.1 T, chosen to permit current drive (CD) via 2.45 GHz microwave sources. This simple design is prone to single point failure (particularly at any of the several soldered joints), was not designed to tolerate quenches, and was operated considerably below the critical current which is ~1 kA at 20 K and in the low self-field which is <1 T at the inner TF limb. A high performance fusion ST will need a TF of 3–4 T, which requires the development of high current HTS cables. TE is currently developing HTS cable, joint and quench management technologies required to build and operate a larger device that will operate at higher field and with very large stored energy (section 3.4). A major challenge is the design of the central column, and this is being addressed in the design work for ST135 (section 4.1).

3.3. ST40

To date STs have operated at TFs of less than 1 T. For high fusion performance, devices operating at 3 T or above will be needed. To construct an ST that can operate at fields at this level, innovative engineering solutions will be needed especially for the central column. To develop and demonstrate solutions to the key engineering aspects, TE is constructing a device (ST40) with copper magnets that is intended to operate at fields up to 3 T. Beyond this device TE is planning high field STs using HTS. ST40 (figure 3), will have a design field of $B_{T_0} = 3$ T at major radius of $R_0 = 0.4$ m, and a centre-rod current of 6 MA. Use of copper for the TF coil (as in all existing STs, except ST25HTS at TE) has the advantages of combining structural strength with good conductivity (especially when cooled to liquid nitrogen temperature). Whereas existing STs have operated typically at 0.3–0.5 T, with the recent MAST, Globus-M and NSTX upgrades striving for 1 T, innovative design features are employed to enable ST40 to operate at up to 3 T. Principal amongst these is the use of Constant Tension Curve TF limbs, specially designed so that over the permitted temperature rise (whether starting from ambient or from liquid nitrogen temperature) the expansions of the centre post and the return limbs are matched, so that minimal movement occurs at the critical top and bottom joints, a simple robust flexi-joint being provided to accommodate the movement.

At fields of 3 T, stresses are high; and an external support structure based on two steel rings (shown in grey above and below the magnet) accommodates in-plane and out of plane forces, such as those arising from tolerance errors in the radial position, and the JxB twists arising from TF-PF and TF-solenoid interactions. The ST40 mechanical design was analysed extensively by a series of electromagnetic analyses using Opera [10], which simulated the forces expected in operational scenarios, including Vertical Displacement Events. These forces were then used in mechanical Finite Element Analyses of major components, using Ansys [11]. For example the central column of the TF magnet, formed from 24 twisted wedge-shaped conductors, exhibits highest stress at the inner edge. For the maximum wedge current of 0.25 MA required to produce a field of 3 T at plasma major radius of 0.4 m, this stress is ~100 MPa in the copper. The copper is half hard, with a yield stress around 180 MPa. Comparing this to the Von Mises yield criterion gives a factor of safety on yield of 1.8.

An important aid to obtaining such a high field is the use in ST40 of a minimal solenoid, made possible by the merging-compression (MC) process for plasma start-up. This should produce hot plasmas with currents of up to 2 MA without use of the central solenoid, which is only needed to maintain the flat-top current—assisted by the high bootstrap fractions expected, and CD from NBI or RF. Hence, the solenoid is considerably smaller than in MAST and NSTX and their upgrades. This reduces JxB twisting stresses, allows more

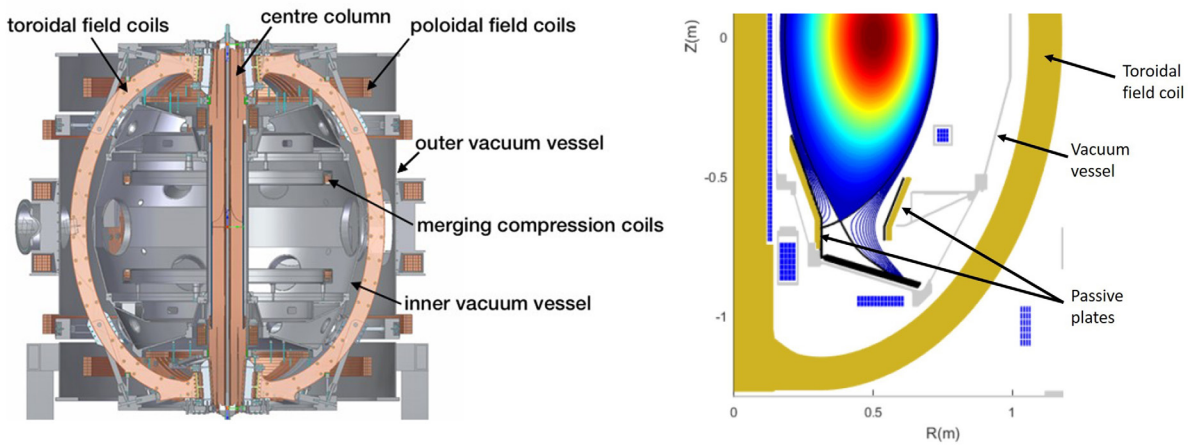

Figure 3. Left: engineering drawing of ST40, showing the steel support rings above and below the vessel, and the merging-compression coils which provide an initial high current, hot plasma without need of the central solenoid. Right: model of the vacuum vessel and components of ST40. KINX simulations show [9] that growth rates of the highly elongated ($\kappa \sim 2.6$) plasma shown can be limited to e-fold times of ~20 ms by the passive plates (indicated), and can be stabilized by internal active feedback coils.

copper for the TF column which reduces TF resistance and heating, and provides a stronger TF post.

The centre post is constructed from 24 wedges, each twisted by 15 degrees over their length thus obviating the need for a TF compensating coil. The TF, solenoid and PF coils are powered by 'Supercapacitors' such as the Maxwell 125 V, 63 F, 0.5 MJ transport module, providing a very economic power supply from laboratory power supplies. Each unit has a limiting fault current ~7 kA even under dead short conditions providing safety; an important consideration in a 100 MJ capacitor bank. The plasma pulse length is limited by the temperature rise in the centre post; initial operations with a water-cooled TF magnet will provide a TF of 1–2 T at $R_0 = 0.4$ m with a flat top of 1–3 s; operation with liquid nitrogen cooling considerably reduces resistance and hence heating and enables longer pulses, and should permit operation at up to 3 T with a flat top of ~1 s.

The MC coils (indicated in figure 3) operated successfully in START and MAST, and extrapolation to ST40 is discussed in [12]. The MC process involves the formation of plasma rings around each of the MC coils shown in figure 3 by rapid discharge of high voltage capacitor banks. These plasma rings attract each other and merge on the midplane, followed by an adiabatic compression of the plasma to the desired major radius of ~0.4 m. It is shown that plasma current immediately after merging increases with TF and linearly with MC coil current. In ST40 the TF and MC coil current are increased over those in MAST by factors of up to 6 and 2 respectively. Extrapolation indicates ST40 should have plasma current after merging of around 1 MA; the subsequent adiabatic compression phase halves the radius in ST40 and should approximately double the plasma current, assisted by the significant reduction in inductance of the plasma ring as it takes up the highly shaped ST form. The MC scheme will be operated at the highest performance permissible, to produce the highest possible plasma currents and plasma temperatures. The final design features MC coil currents of 600 kAt in each coil, produced by a 11 kV, 28 mF capacitor bank, with a downswing time of ~10 ms which induces the plasma rings, and uses very slender support legs (to minimise interference with the plasma rings which have changing helicity). The MC coil mounting structure was analysed in Ansys, and a prototype was tested to 10 000 cycles at the design load of 73 kN, and then finally pulled to destruction. Final failure occurred at approximately 3 times the design load.

In addition to the original objective of providing a high vacuum version of the pioneering START ST at a tenfold increase in TF, the specification has been extended: indeed, it is expected that the MC scheme will provide up to 10 keV plasmas in ST40, the plasma being heated by the rapid conversion of magnetic field energy into plasma kinetic energy during the merging. Full details of its predicted performance, and of the expected evolution of electron and ion temperature profiles are provided in [12], based on extensive studies on both MAST and Japanese STs in collaboration with Y Ono and his team [13]. The ST40 device is currently under construction and is expected to begin operation in 2017.

3.4. Future development programme

As mentioned above, the intention is to combine the experience gained with the low field HTS device ST25(HTS) with that obtained with the high field copper device ST40 to design and construct high field STs using HTS for the magnets. The objectives will be to develop physics understanding of a high field ST, to test HTS cable technology, and to establish HTS performance during DT fusion conditions. ST40 should provide valuable information to determine energy confinement scaling in a high-field ST. TE is designing a high field HTS magnet, using cable technology similar to that described in section 4, to establish the engineering viability. Research is advancing rapidly on these topics, both in-house and worldwide, and the precise DT fusion experiments are still under consideration. As shown in section 4.3 these can range in size from small short pulse research devices, to steady state devices of major radius ~2 m.

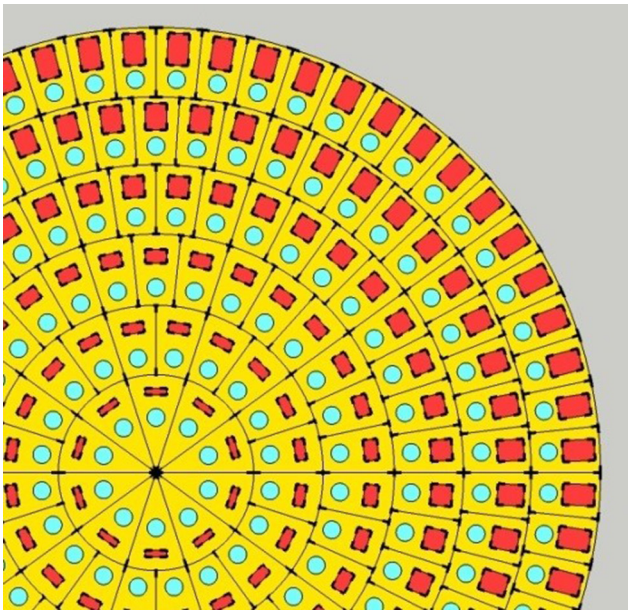

Figure 4. Example of a monolithic HTS centrepost. Orange rectangles represent cables of HTS tapes; blue circles the cooling tubes; yellow areas copper for support and quench protection. In this model, the number of HTS tapes in each cable is chosen to provide constant current density

4. Conceptual design of a prototype fusion power module: ST135

While from a physics perspective it seems that a compact fusion module may be possible (section 2), the feasibility of such a device depends critically on there being satisfactory engineering solutions in a few critical areas. Three important components are the central column where it is necessary to handle the stress in this component at the same time as accommodating the HTS TF magnet; the divertor where it is necessary to handle high power loads; the inboard shielding which is needed to protect the HTS tape from bombardment from high energy neutrons so that it has an acceptable lifetime, and also to reduce the neutron heating to a level that can be handled with a reasonable cryogenic system. Possible solutions for these components are under study and development within TE, and are outlined in the following sections.

4.1. HTS central column design

One possible arrangement (figure 4) utilises two significant features of HTS tape: namely, operation at 20–30 K that gives sufficient current carrying capability at high magnetic field, but at much lower cryogenic cooling cost than operation at 4 K, and the property that tape aligned parallel to the local magnetic field can carry several times more current than non-aligned tape. In this simple model the individual HTS tapes are bonded into multi-layer cables, and for the initial calculations we assume that the entire structure has the strength of half-hard copper.

Towards the geometric centre of the column, the magnetic field reduces and in consequence the current carrying capacity of the HTS tape increases. This makes it possible to reduce the number of tapes. For this simplified design, in which the HTS cables are arranged to produce a uniform current density over the central HTS magnet, we can derive a simple expression for the peak stress which is at $r = 0$, as follows.

Current density in the centre rod magnet is $J_{cc} = I_{cc}/(\pi \cdot R_{cc}^2)$ where I_{cc}(MA) is the total centre rod current, and R_{cc}(m) is the radius of the magnet. Since we are assuming constant current density in the central column, the TF in Tesla at any radius $r(m)$ within it is $B(r) = 0.2\, r\, I_{cc}/R_{cc}^2$. If we neglect hoop stress and integrate the $J \times B$ force from r to R_{cc} we can obtain the inward force at any radius within the central column. We find that the peak compressive stress (σ_{cc}) occurs at the column axis, and is

$$\sigma_{cc} = 0.25\pi B_{T_0}^2 \left(R_0\ R_{cc}^2\right)^2 \text{MPa} \qquad (1)$$

where we have used Ampere's law $B_{T_0} = 0.2\, I_{cc}/R_0$ to replace I_{cc}, where B_{T_0} is the TF in Tesla at the plasma major radius $R_0(m)$.

For the reference ST135 design, $R_0 = 1.35$ m, $R_{cc} = 0.25$ m, plasma current = 7.2 MA, $B_{T_0} = 3.7$ T, $A = 1.8$, elongation $\kappa = 2.64$, and so the peak field at the edge of the HTS magnet is 20 T and the central column current is 25 MA. With a neutron shield thickness of 0.35 m, the calculated peak radial stress is 320 MPa. This is high but is in the form of uniform hydrostatic compression when an axial compressive stress of the same order is provided (below).

A finite element analysis of the centre column with a Young's modulus of 90 GPa and Poisson's ratio of 0.35 gives a peak stress of 255 MPa. This lower figure reflects the support provided by tangential stiffness. However a practical centre column containing cooling channels and various materials with different mechanical properties is likely to have higher localised stress. We find expression (1), although approximate, useful for scoping studies.

Expression (1) shows that forces increase as the square of the TF, but reduce as the square of the central column radius. Hence for example, a 0.05 m addition (20%) to the HTS core radius (accompanied by a 0.05 m decrease in shield thickness, if it is desired to maintain the aspect ratio of 1.8), reduces the field at R_{cc} to 16.7 T and the peak stress to 205 MPa whilst maintaining a field of 3.7 T at $R_0 = 1.35$ m.

Other stresses are also important: in particular, stresses arising from axial loads at the inboard TF leg are considerable and can be the limiting stresses [14] depending on the device design. These stresses are not yet included in our analysis. The compact radial build of an ST module, however, should make it feasible to include an external mechanical structure to apply a pre-load compression of the centre-rod. If this can be accomplished successfully, then the compressive stress would dominate. As a point of comparison, we note that Ignitor has developed a design solution along these lines [15]. In that case, the necessary mechanical strength has been obtained by designing the copper coils and its steel structural elements (C-clamps, central post, bracing rings) in such a way that the entire system, with the aid of an electromagnetic press when necessary, can provide the appropriate degree of rigidity to the central legs of the coils to handle the electrodynamic stresses, while allowing enough deformation to cope with the rapid

thermal expansion of the short pulse machine. The compact aspect of an ST should make a similar approach possible.

Whereas it is conventional to twist superconductor cables to minimize AC losses these will not be significant in the TF magnet of an ST power plant as this will have a slow rise to reach a constant peak current. With a suitable design, use can be made of the substantial increase in performance afforded by aligned operation, giving a corresponding reduction in cost.

4.2. Divertor loads

High power plasmas in relatively small devices would impose high divertor loads if operated in the single-null (SN) configuration, especially in an ST where the inner strike point is at low radius, and space to mitigate the power load by angled strike points or long divertor legs is limited. However the use of double-null divertor (DND) operation, as studied extensively on the START and MAST STs [16], can considerably improve the loading, as the DND configuration is very favourable for the ST concept. Firstly, the inner SOL is now (largely) isolated from the outer, and it is found that most scrape-off-layer (SOL) power escapes through the outer segment and so is incident on the outer strike points; the inner/outer power ratio varies widely, dependent on plasma conditions. During ELMs the ratio can be over 20 times higher; during inter-ELM periods when the core heating is partially retained, the ratio can fall to 4, approximately the ratio of the inner and outer SOL areas; but the average ratio is typically taken as 10 in MAST [17].

Full analysis of the divertor performance requires exact specification of the machine parameters and the detailed divertor design. These details are not available at the present, pre-conceptual phase of the ST135 project. Instead, it is instructive to compare our divertor with the FNSF design [3] that is similar to ST135. FNSF is particularly relevant because an HTS version of the (copper magnet) FNSF series was developed as a joint study between TE and PPPL, and is presently used as a concept design for ST135, as reported in [18]. The study of divertor loads in an $R_0 = 1.7$ m version of FNSF [3] estimates the peak divertor loads for both the inner and outer DND strikepoints to be less than 10 MW m^{-2}. The load on the divertor target is roughly $P_{\rm div}/S_{\rm w}$, where $P_{\rm div} = P_{\rm SOL} - P_{\rm rad}$ is the power delivered to the targets and $S_{\rm w} \propto R_{\rm trg} \times f_x \times \lambda_q$ is the effective wetted area. Here $P_{\rm SOL}$ is the power entering the scrape-off layer (SOL); $P_{\rm rad}$ the power spread over the side walls, mostly by radiation; $R_{\rm trg}$ is the radius of the strike point; f_x the flux expansion from the midplane to the target and $\lambda_{\rm q}$ represents the width of the SOL at the midplane as given by Eich scaling [19]. In reality, $S_{\rm w}$ includes also flux broadening and non-proportional power dissipation in the divertor, but for first estimates one can consider them proportional to λ_q.

ST135 is designed to have $P_{\rm fus} = 200$ MW and $Q_{\rm fus} = 5$, whereas the FNSF design envisages $P_{\rm fus} = 160$ MW and $Q_{\rm fus} = 2$. The heat entering the plasma is the combination of alpha heating and auxiliary heating, making a total of 112 MW in FNSF and 80 MW in ST135, and after radiation losses due to impurity, Bremsstrahlung and cyclotron radiation this will enter the SOL. The strike points $R_{\rm trg}$ are at about 20% larger radius in FNSF and expansion f_x should be very similar. The Eich scaling predicts λ_q varying as $B_{\rm pol}^{-1.2}$ and $B_{\rm pol}$ is a factor 1.4 higher in FNSF, so λ_q is a factor 1.5 larger in ST135. Overall, we conclude that the strike areas should be similar; and since $P_{\rm sol}$ is approximately 30% less, the peak power on each outer divertor in ST135 should be ~7 MW m^{-2} compared to ~10 MW m^{-2} in FNSF. This estimate suggests that the power loading of the divertor targets in ST135 should be tolerable. However the effectiveness of DND operation in limiting inner strike point loads, especially if fast transients such as ELMs are present, is important and requires further experimental results on position control, ELM mitigation, timescales of load transients, etc. Experiments on ST40 are planned to deal with some of these aspects. Other key engineering aspects, such as the parallel heat flux and manufacturing and installation accuracies of the divertor tiles also need investigation.

4.3. Shielding, energy deposition, neutron flux and damage in the central core

An extensive investigation of candidate materials for the inner shield has been carried out and tungsten carbide with water cooling has been identified as a promising material [20]. MCNP Monte Carlo Code [21] calculations of the attenuation due to this shield have been carried out. The attenuation of the neutron flux, and associated heat deposition in the central core, as a function of shield thickness have been parameterised and included in the TE System Code [20]. The heat deposited will have to be removed actively with a cryoplant and an estimate of the power requirement is also included. To determine the optimum shield thickness several factors have to be taken into account simultaneously. For a device of given $Q_{\rm fus}$, H factor and aspect ratio A, it is necessary to consider each of the attenuation due to the shield, the magnetic field on the HTS tape and the radial stress in the central column. The TE system code has been extended so that these different aspects can be considered simultaneously. It was found that in order to keep the peak radial stress around its limiting value of 320 MPa as the major radius increased, the radius of the superconducting core also needed to increase but less rapidly than the shield thickness increase. The extra space in the radial build as the major radius increases is used to increase both the thickness of the shield and of the HTS core in the ratio: 92% to shield thickness $T_{\rm shield}$, 8% to the HTS core radius $R_{\rm cc}$ which approximately maintains constant stress. As an example, for a reference plasma ($Q_{\rm fus} = 5$, $P_{\rm fus} = 201$ MW, H(IPB98y2) = 1.9, $A = 1.8$, $\kappa = 2.64$, βN = 4.5), we present in figure 5 the variation of key parameters with major radius.

We see that at the reference major radius for ST135 ($R_0 = 1.35$ m), the shield thickness is 0.31 m, the field on the conductor is 20.2 T, the plasma current is 7.2 MA, the neutron heating to the central column is 97.7 kW, and the wall load is 1.88 MW m^{-2}. To handle this level of neutron heating we estimate that a cryogenic plant of 3.0 MW wall-plug power would be needed. It is clear from the figure that as the shield thickness increases the heating of the central column reduces rapidly.

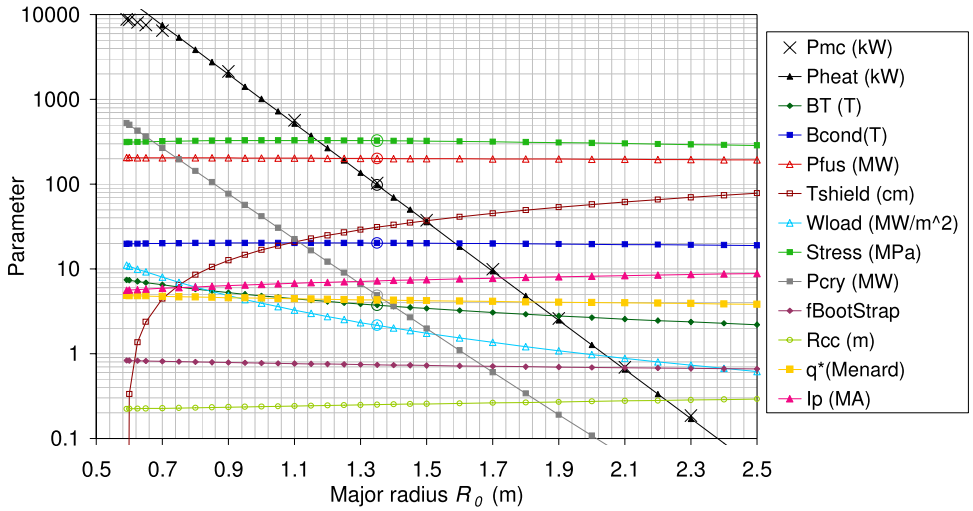

Figure 5. Heating power deposited in the superconducting core, and other key parameters, as a function of plasma major radius. The scan has been performed with a constant $H_{\mathrm{IPB98y2}} = 1.9$, the central temperature adjusted to give 0.8 of the Greenwald density limit, and the TF adjusted to give 0.9 of the beta limit. The extra space made available by increasing the major radius has been divided in the ratio 92% to the shield thickness T_{shield} and 8% to the HTS core radius R_{cc} across the plot. The circles show the reference design at 1.35 m major radius. The crosses show the energy deposition calculated independently using the MCNP code.

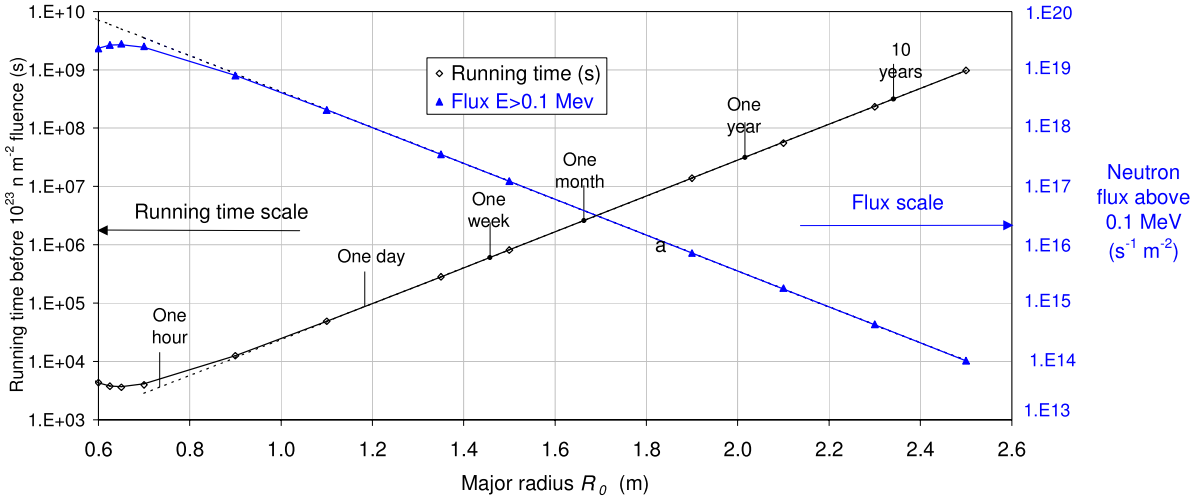

Figure 6. The neutron flux across the outer surface of the mid-plane region of the superconducting core for neutron energies above 0.1 MeV is shown by the full blue triangles (right-hand scale). The number of seconds of continuous running which correspond to a total neutron fluence of 10^{23} m^{-2} are shown by the open diamonds (left hand scale). The dashed lines are fitted exponentials with a slope 7.0833 m^{-1}. The blue line is a fit to the flux distribution and the black line the corresponding running time.

Using expression (1), the peak stress in the central column is 326 MPa. From the comparison with FNSF (section 4.2) the peak divertor load would be ~7 MW m^{-2}. For all values of R_0, q^*(Menard) defined as $5 \times (1 + \kappa^2)/2a^2B/(RI)$ is $\geqslant 2.8$, the value recommended for avoidance of disruptions in NSTX [3].

The crosses in figure 5 show computations of the energy deposition into the superconducting core made using the MCNP code. It is seen that the fit to the System Code prediction is good over a wide range of radius without the need for any change in parameters. The left of the figure corresponds to the limit of zero shield thickness and it is seen that only here, for shield thickness below a few cm, that the computed deposited power falls significantly below the simple exponential dependence of form $10^3 \times \exp[-6.61(R_0 - 1.35)]$ kW (where R_0 is in m). A key aspect not yet included is any change in tape performance due to irradiation by neutrons. The neutron flux across the outer surface of the superconducting core has been calculated using MCNP. The full triangles in figure 6 show the neutron flux above 0.1 MeV for the outer surface of the superconducting core as measured in the central mid-plane region (8.6% of the total core height) where the flux is highest. The flux variation with major radius fitted at larger radii above 1 m is shown by the dashed lines to decay exponentially appreciably faster than that for the power deposition mentioned earlier with a form $3.54 \times 10^{17} \exp[-7.08(R_0 - 1.35)]$ n s^{-1} m^{-2}. It is seen that for lower major radii below 1 m the flux is rather lower than predicted from the exponential decay. Indeed for zero shield thickness, which occurs at major radius 0.592 m, the flux is only a fraction 0.283 of its expected value. This is modeled as shown in the full lines by subtracting from the above function $5.45 \times 10^{19} \exp[-14.56(R_0 - 0.592)]$.

Inevitably the HTS performance will degrade but information on the extent of the degradation is limited. Eisterer's work on HTS tapes [22] irradiated in a fission reactor has suggested that the tape lifetime corresponds to a total neutron fluence of about 10^{23} m^{-2}. The open diamonds in figure 6 show the seconds of continuous running assuming this fluence limit. For many scientific objectives, the actual running time is likely to be composed of many relatively short pulses.

The measurements by Eisterer were made at ambient temperatures rather than ~30 K as expected during operation. They were made using a reactor flux whose energy dependence may be quite different from that expected behind the neutron shield of a fusion plant. Gamma radiation damage has not been included and may be important. Raising the temperature of the tape temporarily (annealing) may restore tape performance. In this case also information is limited and dedicated R&D is needed.

5. A modular power plant

If a relatively small fusion module is feasible, then a possible alternative supply of fusion power based on a modular concept may be available. Compared to ST135, a higher $Q_{\rm fus}$ would be needed, ~10–20, and the tritium breeding ratio would need to be >1. To meet these requirements, the device would probably have to be somewhat larger than ST135 but still small relative to the large DEMOs considered for the single device approach. The energy confinement in STs at high field, and the thickness of shielding needed to protect the HTS, especially on the central column, have a strong impact on the minimum size. It is expected that within the next few years better estimates in both cases will be available through dedicated R&D and it will be possible to optimise the size and power of a ST fusion module. The economics and operational advantages of a modular concept, utilizing perhaps 11 small 100 MW units, (10 working and 1 undergoing maintenance) have already been outlined [23]. The advantages include improved availability; cyclic maintenance; the need for only a relatively small hot cell; a sharing of start-up and energy conversion facilities; the possibility of providing plant output varying in time by switching individual modules, and the economics of mass-production. STs can exhibit the combination of high bootstrap fraction and high beta-important both for maximizing power gain and in obtaining/maintaining the plasma current, especially in the absence of a central solenoid. In this latter respect, recent predictions that RF techniques can provide full plasma current initiation and ramp-up [24] are encouraging; initial tokamak-like plasma can be formed by using electron Bernstein wave (EBW) start-up alone [25]. Then EBW CD may be used further for the plasma current ramp-up because of its relatively high efficiency $\eta = R_0 n_e I_{\rm CD}/P_{\rm RF} \approx 0.035$ (10^{20} A W^{-1} m^2) [26] at low electron temperatures. EBW CD efficiency remains high even in over-dense ($\omega_{\rm pe} > \omega_{\rm ce}$) plasma [27]. At the reactor level of temperatures ~10 keV, EBW CD efficiency $\eta \approx 0.1$ would become compatible with other CD methods so a combination of different CD techniques with different accessibilities to the plasma may become beneficial.

6. Summary

The TE programme is aimed at developing the ST as a future power source. Areas that have a high leverage on the feasibility of this approach have been identified and are under study in current R&D. Two such areas are the energy confinement scaling at high field (3–4 T), and the impact of fusion neutron irradiation on the properties of HTS rare earth tape at 20–30 K. Both are under investigation and the data should be available in the near future. Favourable results could lead to economic fusion based on modular high gain STs of relatively small size ($R_0 < 1.5$ m); less favourable results could lead to larger but still economic ST fusion power plants of around 1.5–2 m major radius. In either case, the small scale of the fusion modules should lead to rapid development and make possible the resolution of the remaining key outstanding physics and technology steps that are needed for the realisation of fusion power.

References

[1] Peng Y-K.M. and Strickler D.J. 1986 Features of spherical torus plasmas *Nucl. Fusion* **26** 769
[2] Sykes A. *et al* 1999 The spherical tokamak programme at Culham *Nucl. Fusion* **39** 1271
[3] Menard J.E. *et al* 2016 Fusion nuclear science facilities and pilot plants based on the spherical tokamak *Nucl. Fusion* **56** 106023
[4] Ono M. and Kaita R. 2015 Recent progress on spherical torus research *Phys. Plasmas* **22** 040501
[5] Sorbom B.N. *et al* 2015 ARC: A compact, high-field, fusion nuclear science facility and demonstration power plant with demountable magnets *Fusion Eng. Des.* **100** 378–405
[6] Costley A.E., Hugill J. and Buxton P.F. 2015 On the power and size of tokamak fusion pilot plants and reactors *Nucl. Fusion* **55** 033001
[7] Petty C.C. 2008 Sizing up plasmas using dimensionless parameters *Phys. Plasmas* **15** 080501
[8] Sykes A. *et al* 2014 Recent advances on the spherical tokamak route to fusion power *IEEE Trans. Plasma Science* **42** 482–8
[9] Gryaznevich M.P. *et al* 2016 Overview and status of construction of ST40 IAEA CN-234 *2016 IAEA Fusion Energy Conf., paper FIP/P7-19 (Kyoto)* https://conferences.iaea.org/indico/event/98/session/31/contribution/509
[10] Opera finite element Simulation Software www.operafea.com/
[11] Ansys software http://www.ansys.com/en-GB
[12] Gryaznevich M.P. and Sykes A. 2017 Merging-compression formation of high temperature tokamak plasma *Nucl. Fusion* **57** 072003
[13] Ono Y. *et al* 2015 High power heating of magnetic reconnection in merging tokamak experiments *Phys. Plasmas* **22** 055708
[14] Morris J. *et al* 2015 Implications of toroidal field coil stress limits on power plant design using process *Fusion Des. Eng.* **98–9** 1118–21
[15] Bombarda F., Coppi B., Airoldi A., Cenacchi G. and Detragiache P. 2004 Ignitor: physics and progress towards ignition *Braz. J. Phys.* **34** 1786–91
[16] Counsell G.F. *et al* 2002 Boundary plasma and divertor phenomena in MAST *Plasma Phys. Control. Fusion* **44** 827–43
[17] Harrison J.R., Fishpool G.M. and Kirk A. 2013 L-mode and inter-ELM divertor particle and heat flux width scaling on MAST *J. Nucl. Mater.* **438** S356

[18] Brown T., Menard J., El Guebaly L. and Davis A. 2015 PPPL ST-FNSF engineering design details *Fusion Sci. Technol.* **68** 277–81
[19] Eich T. *et al* 2013 Scaling of the tokamak near the scrape-off layer H-mode power width and implications for ITER *Nucl. Fusion* **53** 093031
[20] Windsor C.G., Morgan J.G. and Buxton P.F. 2015 Heat deposition into the superconducting central column of a spherical tokamak fusion plant *Nucl. Fusion* **55** 023014
[21] Goorley T. *et al* 2012 Initial MCNP6 release overview *Nucl. Technol.* **180** 298–315
[22] Prokopec R., Fischer D.X., Weber H.W. and Eisterer M. 2014 Suitability of coated conductors for fusion magnets in view of their radiation response *Supercond. Sci. Technol.* **28** 014005
[23] Gryaznevich M.P., Chuyanov V.A., Kingham D., Sykes A. and Tokamak Energy Ltd 2015 Advancing fusion by innovations: smaller, quicker, cheaper *J. Phys.: Conf. Ser.* **591** 012005
[24] Raman R. and Shevchenko V. 2014 Solenoid-free plasma start-up in spherical tokamaks *Plasma Phys. Control. Fusion* **56** 103001
[25] Shevchenko V. *et al* 2010 Electron Bernstein wave assisted plasma current start-up in MAST *Nucl. Fusion* **50** 022004
[26] Shevchenko V. 2002 Generation of noninductive current by electron-Bernstein waves on the COMPASS-D tokamak *Phys. Rev. Lett.* **89** 265005
[27] Laqua H.P. *et al* 2003 Electron-Bernstein-wave current drive in an overdense plasma at the Wendelstein 7-AS Stellarator *Phys. Rev. Lett.* **90** 075003